Comparative study of stabilization/solidification of dredged sediments with ordinary Portland cement and calcium sulfo-aluminate cement in the framework of valorization in road construction material

R. Zentar, Hongwei Wang, Dongxing Wang

Comparative study of Stabilization/Solidification of dredged sediments with Ordinary Portland cement and Calcium Sulfo-Aluminate cement in the framework of valorization in road construction material

Rachid ZENTAR[a,b], Hongwei WANG[a,b,c*], Dongxing WANG[c*]

[a] IMT Lille Douai, Institut Mines-Télécom, Center of Materials and Processes, F-59000 Lille, France.

[b] Univ. Lille, Institut Mines-Télécom, Univ. Artois, Junia, ULR 4515 - LGCgE, Laboratoire de Génie Civil et géo-Environnement, F-59000 Lille, France.

[c] School of Civil Engineering, Wuhan University, 430072 Wuhan, China.

[*]Corresponding authors at: School of Civil Engineering, Wuhan University, 430072 Wuhan, China.

E-mail addresses: whuwhw@whu.edu.cn (H. Wang), dongxing-wang@whu.edu.cn (D. Wang).

Abstract

Stabilization/solidification (S/S) of dredged sediments is an environmentally friendly, low-cost and time-efficient way to manage this waste (according to the European waste classification) in the context of valorization as novel resources. In this study, the main objective was to evaluate the efficiency of using a novel and green binder Calcium Sulfo-Aluminate (CSA) cement to solidified Dunkirk sediments. For comparison, the Ordinary Portland Cement (OPC) binder was used as a reference. For this purpose, several tests were performed on samples containing various types and amounts of binders. The experimental program included: modified Proctor compaction test, immediate Californian Bearing Ratio (I-CBR) index test, unconfined compressive strength test, splitting tensile strength test, measurements of elastic and secant modulus, and mineral and micropore structure analysis. It is realistic to conclude that the compaction performance of the CSA-/OPC-solidified sediments is significantly improved. The mechanical performance of compressive, tensile strength and elastic modulus increases with binder content and curing time. The simple model obtained to relate the compressive and tensile strength with elastic modulus allow predicting easily, for a given suitable set of characteristics, the type or the amount of binder needed. This model allows optimizing the amount of binder to reach a given properties of solidified sediments and hence improves the cost of developed material. The results also demonstrate the ability of solidified sediment to be valorized in road construction.

Keywords: Sediments; Valorization; Ordinary Portland Cement; Calcium

Sulfo-Aluminate cement; Mechanical strength; Road material

1. Introduction

To prevent flood risks and ensure a sufficient draft for navigation, regular sediment dredging is carried out every year. However, the dredging process produce a large amount of sediments. In Europe, the annual volume of dredged sediments is estimated at 300 million tons [1]. Fine dredged sediments is regarded as waste with high moisture content, complex components (as contaminants), high organic matter content, high compressibility and low mechanical strength [2], [3], [4], [5]. Conventional management of sediments as ocean dumping, land deposit, and blow-filled piling, are not sustainable and environmentally friendly as it can cause serious secondary pollution [6], [7]. Therefore, try to find an alternative method for sediments management is the core of current research.

The valorization of sediments in road construction by stabilization/solidification (S/S) method has received considerable interest in recent years [8], [9], [10], [11], [12]. Stabilization/Solidification (S/S) is considered as an environmentally friendly, low-cost and time-efficient way for the treatment of sediments. It can significantly relieve environmental impacts and improve the mechanical properties of sediments [13]. The reuse of S/S treated sediments in the field of construction can be considered as a promising method not only to solve problems related to sediment management but also to provide a new source of construction materials [14], [15]. The traditional binder used for S/S is Ordinary Portland Cement (OPC), and the justification has been proved by efficiency shown over time, low cost, availability and reliability [16], [17].

However, the manufacturing process of OPC has significant environmental issues, i.e., high consumption of energy (5000 MJ/t cement), non-renewable resources (1.5 t limestone and clay/t cement) and high CO_2 emissions (0.95 t CO_2/t cement). OPC manufacturing acts as a significant contributor to anthropogenic CO_2 emission (5-7 %) [18], [19]. Due to the increasing demand for construction, the share of CO_2 emissions attributed to the cement production is predicted to increase from 16 % to 24 % by 2050, demonstrating the urgent need to improve its sustainability [20]. Therefore, several research works are undertaken to propose alternative cementitious material with low energy consumption, less pollution or no pollution and excellent durability, such as reactive MgO [21], magnesia–industrial by products [22], [23], [24], Si-modified MgO cement [16], industrial by products–cement [17], calcined dredging sediments–cement [25], basalt fiber–cement [26] uncontaminated sediments–cement [27] and others.

The continuous push toward the development of a sustainable cementitious binder has resulted in increased research activity on Calcium Sulfo-Aluminate (CSA) cement in the last few decades. CSA cement is produced by the calcination of gypsum, bauxite, and limestone at ~1250 °C, which is 200 °C lower than the temperature used for Portland cement clinker (~1450 °C) [28]. Moreover, the lower limestone demand (35 % - 40 %) for the manufacture of CSA cement reduces its carbon footprint. The production of 1 t of OPC clinker releases a maximum of 0.95 t of CO_2, whereas the production of 1 t of CSA clinker leads to reduce by one third the CO_2 emissions [29], [30]. The main hydraulic phase of CSA is ye'elimite (C_4A_3S), and the secondary

89 phases included belite (C_2S), calcium sulfate, and gehlenite (C_2AS), etc. The
90 hydration of ye'elimite is used to gain early age strength, and the hydration of belite
91 could improve long-term strength [31], [32]. CSA cement exhibits many interesting
92 properties such as short setting time, high early strength, impermeability, sulfate, and
93 chloride corrosion resistance, and low alkalinity [32], [33], [34], [35]. Hence, CSA
94 cement has demonstrated considerable potential in the S/S of hazardous materials,
95 such as low-level radioactive waste, heavy metals waste, sewage sludge, bottom ash,
96 and galvanic sludge [36], [37], [39], [40], [41]. Besides, a few studies use CSA
97 cement in geotechnical applications, especially in ground improvement. For example,
98 it is proved that CSA-treated sand has significantly high initial strength, which
99 powerfully indicates that the use of CSA in geotechnical applications may lead to the
100 reduced construction period and carbon footprint [42], [43], [44], [45]. In fact, to the
101 best of our knowledge, there remain scientific questions as to reused sediments with
102 CSA cement, no research thus far on the use of CSA cement with sediments in road
103 construction. Therefore, this study evaluates the effectiveness of CSA cement on the
104 marine sediment from Dunkirk Port (France) for potential use as road material.
105 In this context, the main objectives of the present research work are: (i) to assess the
106 Proctor compaction properties and immediate Californian Bearing Ratio (I-CBR)
107 index of solidified sediments with the addition of CSA cement; (ii) to validate the
108 efficacy of CSA cement in enhancing the properties (e.g., compressive strength,
109 tensile resistance, and elastic modulus) of solidified sediment and (iii) to demonstrate
110 its ability in comparison to OPC treatment. The results of this paper will contribute to

111 an investigation on the feasibility of using an eco-friendly CSA binder and dredged
112 marine sediments as road material products without complex treatment.
113
114 **2. Experimental materials and methods**
115 **2.1. Raw Materials**
116 The sediments (SD) were dredged from Dunkirk Harbour in the north of France. The
117 basic physical characteristics of sediments are measured according to the standard
118 used in France and/or Europe.
119 - The initial water content is measured according to test standard NF P 94-050
120 [46].
121 - The true density is measured using a helium pycnometer (NF EN ISO 17892-3)
122 [47].
123 - The organic matter is measured by the ignition method at 450 °C (XP P94-047)
124 [48].
125 - The liquid limit and plastic limit, defined by the percussion-cup method and
126 the rolling thread method is measured according to test standard EN ISO
127 17892-12 [49].
128 - The particle size distribution is measured according to test standard EN ISO
129 13320 [50].
130 In terms of binders, Ordinary Portland cement (OPC) with CEM I 52.5 R from
131 LafargeHolcim Saint-Pierre-La-Cour company and calcium sulfoaluminate cement
132 (CSA) from Vicat company were used in this study. The chemical compositions of all

these materials were determined by X-ray fluorescence (XRF) analysis with a BRUCKER AXS D8 ADVANCE using cobalt and kα radiation (kα=1.78 Å), the results are listed below.

2.2. Methods

In the current study, the mix proportions of different samples are shown in Table 1, which was designed with reference to our previous research [8], [9], [23]. It should be noted that the content of OPC and CSA was determined in percentage by mass of dry sediments. Tap water was used as mixing water.

The modified Proctor compaction tests and immediate Californian Bearing Ratio (I-CBR) index tests were carried out according to NF EN 13286-2 [51] and NF EN 13286-47 [52], to determine the feasibility of the solidified sediments to be used as a filling material in the road. The test carries out in a Proctor mould with a diameter of 150 mm and a height of 120 mm, and the sediment was filled up in five equal layers and 25 strokes were applied to each layer with a 4.5 kg hammer by performing falls from a height of 457 mm. Then test the water content and I-CBR index, in order to determine the maximum dry unit weight, optimum water content and I-CBR index values of the solidified sediments.

The unconfined compressive strength was measured by using the INSTRON testing machine according to NF EN 13286-41 [53], as shown in Fig. 1 (a). The cylindrical specimens were prepared by static compression at their respective maximum dry density and optimum water content, according to NF EN 13286-53 [54]. Firstly, the dry sediments and cement were mixed in an electric mixer for 5 min. Then the tap

155 water was added and mixing is performed for another 5 min. Afterwards, the mixtures
156 were transferred into the cylindrical mould with a diameter of 50 mm and a length of
157 100 mm. By using axial compression, the mixtures is compacted to reach the desired
158 height. The compacted specimen was demolded and stored in covered plastic boxes
159 for preventing the moisture losses. The curing is made in a curing room at 20 ± 1 °C
160 for 3 d, 7 d, and 28 d. A group of three same cylindrical specimens was prepared for
161 each mixes, and the results discussed later were the average values measured on three
162 specimens. The unconfined compressive strength is given by the equation (1).
163 The elastic modulus is determined in an unconfined compression test in accordance
164 with NF EN 13286-43 [55], which using the secant slope at 30% of peak compressive
165 strength. Firstly, the maximum compression strength of the specimen is measured (for
166 a given mix). Then the elastic modulus is measured on another sample. As shown in
167 Fig. 1 (b), to measure the elastic modulus, an extensometer with three displacement
168 sensors were used. During the elastic modulus measurement, the compressive
169 maximum effort applied corresponds to 30% of the maximum compression strength.
170 The elastic modulus is determined according to equation (2).
171 The indirect tensile strength test was chosen so as to obtain the splitting tensile
172 strength, which determined in accordance with NF EN 13286-42 [56]. For the indirect
173 tensile test, the same specimens (ϕ 50 mm × h 100 mm) as those in the unconfined
174 compressive strength test were used. The specimen was placed horizontally between
175 two-plywood band, and a compressive force applied perpendicularly to the axis of
176 symmetry of the cylinder specimen, as shown in Fig. 1 (c)-(d). The splitting tensile

strength is calculated by the following equation (3).

$$q_c = \frac{4F_c}{\pi D^2} \quad (1)$$

$$\mathrm{E} = \frac{1.2F_c}{\varepsilon_E \pi D^2} \quad (2)$$

$$q_{it} = \frac{2F_{it}}{\pi HD} \quad (3)$$

where q_c is the unconfined compressive strength; q_{it} is the splitting tensile strength; F_c is the maximum force of compressive test; F_{it} is the maximum force of tensile test; H and D are the length and diameter of the specimens; ε_E is the longitudinal strain of the specimen, when F = 0.3 F_c.

The crystallographic composition and microstructural properties of typical samples were investigated by X-ray diffraction (XRD) and mercury intrusion porosimetry (MIP) tests. Fragments taken from the broken samples after compressive strength tests were dried at 40 °C for at least 48 h. The XRD analysis was determined by the BRUCKER AXS D8 ADVANCE X-ray diffractometer with a Co Kα radiation source. The micropore structure analysis was defined by the MIP tests with a Micromeritics Autopore V porosimeter.

Table 1 Mix proportions of different samples.

Samples	OPC (%)	CSA (%)	SD (%)	Curing time (d)
SD	0	0	100	3, 7, 28
SD2OPC	2	-	98	3, 7, 28
SD4OPC	4	-	96	3, 7, 28
SD6OPC	6	-	94	3, 7, 28
SD2CSA	-	2	98	3, 7, 28
SD4CSA	-	4	96	3, 7, 28
SD6CSA	-	6	94	3, 7, 28

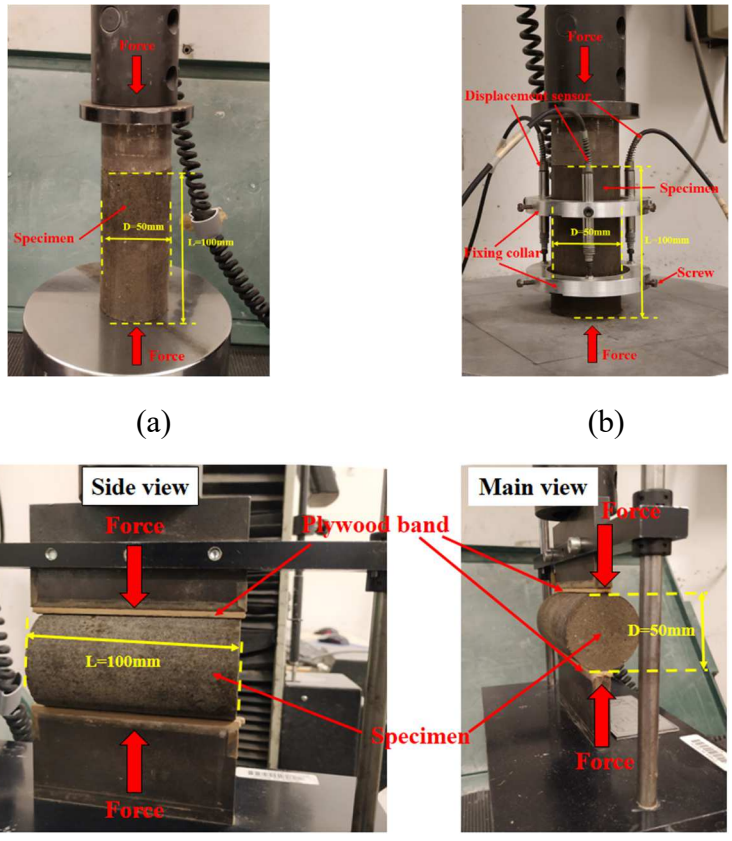

Fig. 1 A view of the (a) unconfined compressive strength and (b) elastic modulus test; (c) The side view and (d) the main view of indirect tensile strength test.

3. Results and discussion

3.1. Physical and chemical characteristics

The basic physical characteristics of sediments are shown in Table 2. The initial water content measured is about 5.20 %. It is worth to note that this value is related to the water content of the sediments after 3 months of natural drying. After dredging this later value can exceed 100 %. The true density, measured using a helium pycnometer is about 2.58 g/cm^3. The organic matter measured by the ignition method is about 7.67 %. The low value of the true density could be explained by the high amount of

organic matter content measured. The liquid limit and plastic limit, defined by the percussion-cup method and the rolling thread method are respectively 39.5 % and 28.0 %. The test results induce a plasticity index of 11.5 %. This result is typical of previous studies on sediments dredged in the north part of France. The results for the particle size distribution show that the sediments are composed of 6.97 % clay, 39.48 % silt and 53.55 % sand. The low proportion of clays particle combined with the high amount of organics matter content could explain the obtained value of liquid limit and plastic limit.

For Ordinary Portland Cement (OPC), Calcium Sulfo-Aluminate cement (CSA) and sediments used in this study, the chemical compositions are listed in Table 3.

Table 2 Basic physical characteristics of sediments.

Parameter	Value	Test standard
Initial water content (%)	5.20	NF P 94-050
Density (g/cm^3)	2.58	NF EN ISO 17892-3
Organic contents (%)	7.67	XP P94-047
Atterberg limit tests		EN ISO 17892-12
Liquid limit (%)	39.5	
Plastic limit (%)	28.0	
Plasticity index (%)	11.5	
Particle size distribution		EN ISO 13320
Clay fraction (% < 2 μm)	6.97	
Silt fraction (2 μm < % < 63 μm)	39.48	
Sand fraction (% > 63 μm)	53.55	

Table 3 Chemical composition of the materials. (wt %)

Components	MgO	Al_2O_3	SiO_2	SO_3	K_2O	CaO	TiO_2	Fe_2O_3
SD	1.5	5.4	51.4	traces	1.2	12.1	0.3	4.9
OPC	1.0	4.8	19.9	3.3	1.0	64.1	0.3	2.6
CSA	1.1	17.4	8.5	13.7	0.3	40.5	0.9	7.3

3.2. Compaction properties and I-CBR Index

The effects of CSA and OPC binders on the compaction curves under the modified Proctor compaction test are shown in Fig. 2. The saturation degree curves for Sr = 80 % and Sr = 100 % are also presented in Fig. 2.

According to European standard NF EN 13286-2 [51], we can easily get the values of maximum dry density and optimum moisture from the Proctor curve, which corresponding to the coordinate of maximum position on the Proctor curve. It can be seen from Fig. 2 that for the raw sediments, the maximum dry density is 1.641 g/cm^3, and the corresponding optimum moisture content is 21.8 %. For solidified sediments with OPC, the maximum dry density is highly reduced after 2 % addition of OPC whereas for 4 % and 6 % addition the changes of dry density are less important (decrease of maximum dry density from 1.578 g/cm^3 to 1.574 g/cm^3). At the same time with the decrease in the maximum dry density, the optimal moisture content increases in the same way. For solidified sediments with CSA, as for OPC addition, the maximum dry density is highly reduced after 2 % addition of CSA and at the same time, the optimal moisture content is increased. However, with an addition of 4 % and 6 % of CSA in the mixture, the maximum dry density seems to increase again and the optimal water content decreases (an increase of maximum dry density from 1.575 g/cm^3 to 1.615 g/cm^3 and a decrease of optimal moisture content from 23.5 % to 20.2 %). These results are well highlighted in Fig. 4 (a)-(c).

Fig. 3 shows the I-CBR index curves of the raw sediments and OPC/CSA-solidified sediments. The measured I-CBR index values at the optimal moisture contents for all

246 the mixtures are shown in Fig. 4 (c). The I-CBR index value of raw sediments is about
247 15 % at the optimum moisture content. This value is lower than that for a sub-layer
248 material (I-CBR ≥ 25 %) according to the specifications in French standards [57]. The
249 addition of CSA to dredged sediments leads to an increase linearly of the I-CBR index
250 with the increase in the CSA content. After the addition of 2 % of CSA, the I-CBR
251 index value reach 20 % at the optimum moisture content and then increases to 30 %
252 and 40 % as the CSA content increases to 4 % and 6 %. From this result, it could be
253 reasonable to predict that the treatment of sediments by 3 % of CSA could be
254 sufficient to reach an I-CBR index value of 25 % with is the due value to be used in
255 sub-layer material (I-CBR ⩾ 25 %). To be used in the foundation layer (I-CBR ⩾
256 35 %), treatment with 5 % CSA could be a reasonable value according to the
257 specifications in French standards [57].
258 For the OPC-solidified sediments, its I-CBR index values increase from 30 % to 45 %
259 with the increase of the OPC content from 2 % to 6 %. From this result, it could be
260 also reasonable to predict that the I-CBR index value of treated sediments with 1.5 %
261 OPC could be sufficient to reach 25 %, which is the due value to be used in sub-layer
262 material (I-CBR ⩾ 25 %). To be used in the foundation layer (I-CBR ⩾ 35 %),
263 treatment with 4 % OPC could be a reasonable content.
264 It appears from these results that some of the solidified sediment specimens (include
265 SD2OPC, SD4OPC, SD6OPC, SD4CSA and SD6CSA) present adequate properties
266 for use as road material. However, the results of modified Proctor and I-CBR index
267 tests reflect the behavior of solidified sediment in a short time (curing for less than 1

hour). To examine the mechanical behavior of solidified sediment in the long term (curing for several days or even longer periods), it is necessary to measure the mechanical characteristics in terms of compressive strength and/or tensile strength and elastic modulus at long terms.

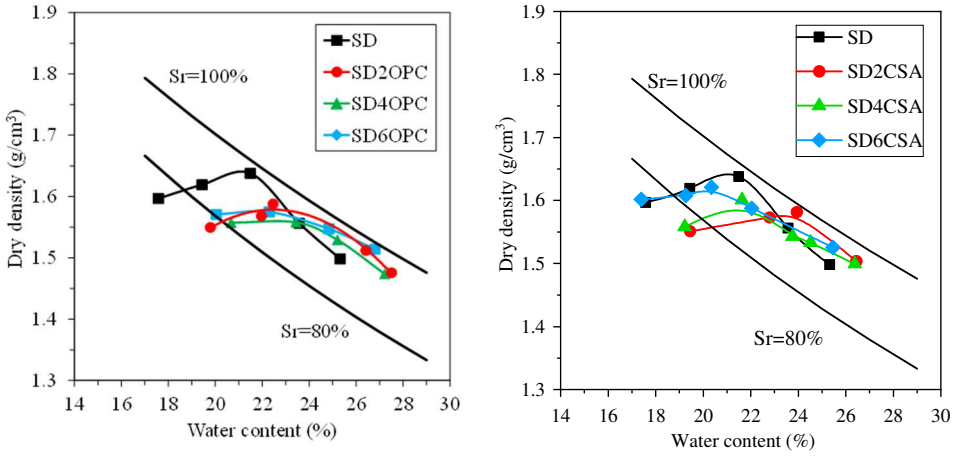

Fig. 2. Compaction curves of solidified sediments with (a) OPC; (b) CSA.

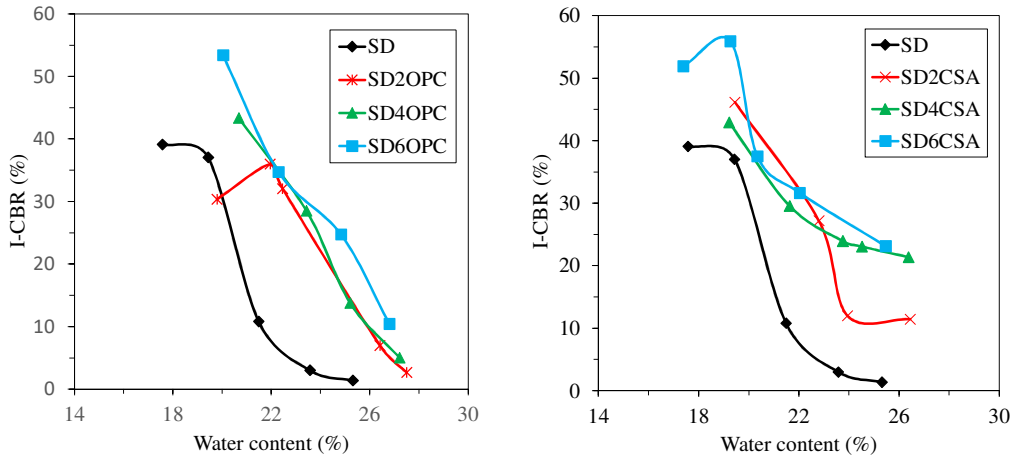

Fig. 3. I-CBR index curves of solidified sediments with (a) OPC; (b) CSA.

281 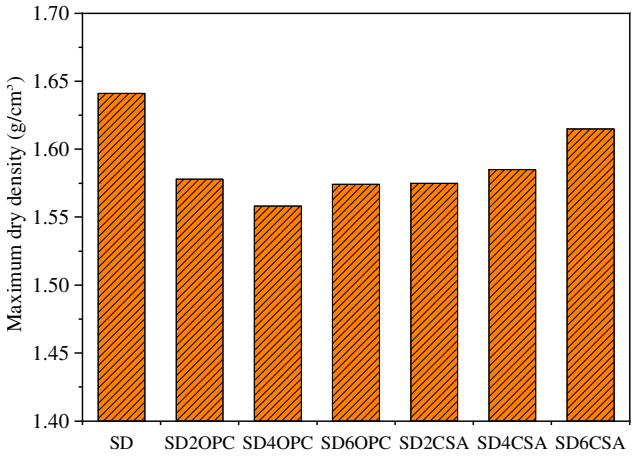

282 (a)

283 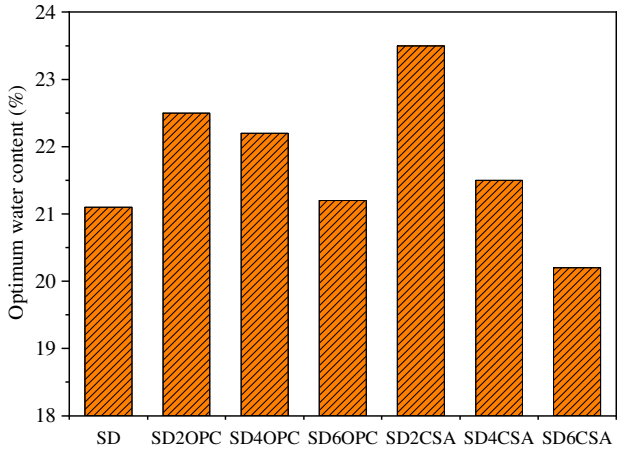

284 (b)

285 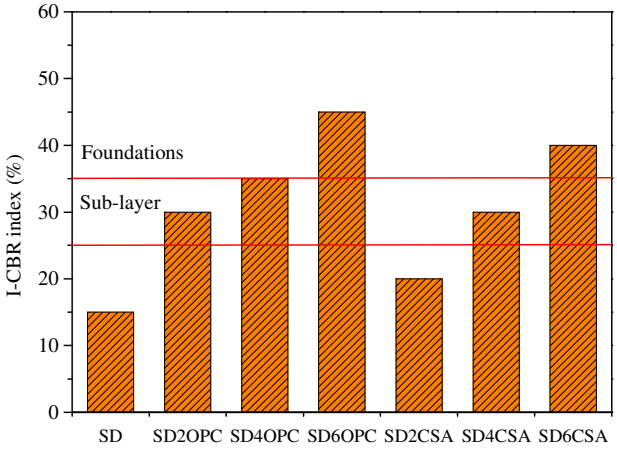

286 (c)

287 **Fig. 4.** (a) Maximum dry density; (b) Optimal moisture content; (c) I-CBR index of

288 different samples.

289

3.3. Unconfined compressive strength

Fig. 5 shows the variation of unconfined compressive strength (q_c) and unconfined compressive strength ratio (η_c, defined as the ration of unconfined compressive strength of solidified sediments q_{cn} to the unconfined compressive strength of raw sediments q_{c0} as in equation (4)) with the amount of treatment with OPC.

$$\eta_c = \frac{q_{cn}}{q_{c0}} \qquad (4)$$

For instance, under the condition of 28 d curing, the raw sediments (SD) display the lowest q_c value (0.50 MPa), and the q_c of solidified sediments with 2 %, 4 % and 6 % OPC inclusion increases to 0.76 MPa (SD2OPC), 1.40 MPa (SD4OPC) and 1.91 MPa (SD6OPC). Meanwhile, the η_c correspondingly increases to 1.52 (SD2OPC), 2.80 (SD4OPC) and 3.82 (SD6OPC) as compared with that of SD (1.00). In addition, under the condition of the 4 % OPC content, the q_c of solidified sediments (SD4OPC) is respectively 1.05 MPa, 1.14 MPa and 1.40 MPa at 3 d, 7 d and 28 d, while the corresponding η_c changes from 2.10 to 2.28 and 2.80. This experimental result is consistent with the previous study performed [9], [11].

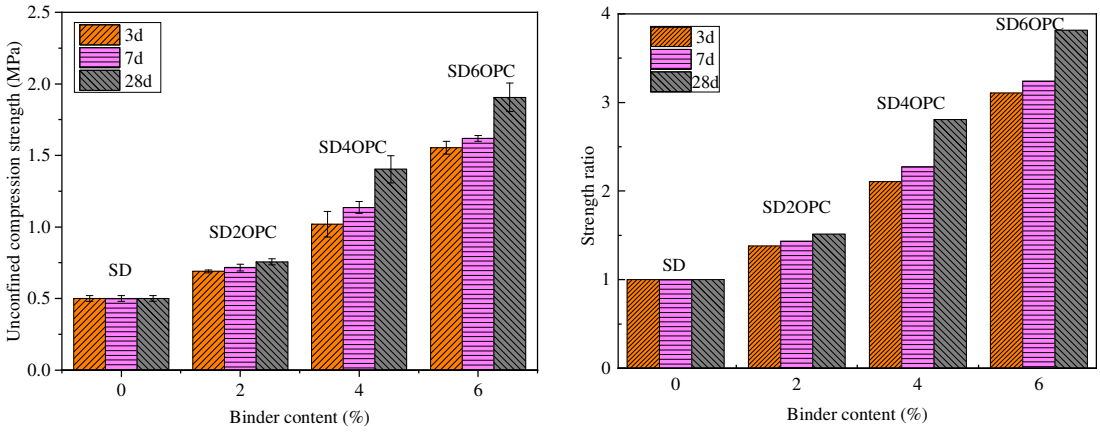

(a) (b)

Fig. 5. (a) Unconfined compressive strength and (b) strength ratio of solidified

sediments with OPC.

For CSA-solidified sediments specimens, the q_c and η_c are reported in Fig. 6. It is similar to OPC-solidified sediments specimens, both CSA content and curing time lead to possibly changing trend of the q_c and η_c. After the same curing time of 28 d, the q_c of CSA-solidified sediments specimens increases from 0.50 MPa (SD) to 0.59 MPa (SD2CSA), 1.20 MPa (SD4CSA) and 1.71 MPa (SD6CSA) with the increase of CSA content from 0 % to 6 %, the η_c correspondingly increases from 1.00 (SD) to 1.18 (SD2OPC), 2.40 (SD4OPC) and 3.42 (SD6OPC). Under the condition of 4 % CSA inclusion, the qc of SD4CSA specimens is 1.04 MPa (3 d), 1.08 MPa (7 d) and 1.20 MPa (28 d) with the curing time changes from 3 d to 28 d, while the corresponding η_c is 2.07 (3 d), 2.17 (7 d) and 2.40 (28 d), respectively.

However, for solidification of sediments as road material, comparing the effects of OPC and CSA treatment under the same condition (binder content and curing time), it can be seen that the CSA performs a little worse than OPC from the point of view of engineering performance capacity. The CSA did not show its high early strength property for solidification of sediments in this study. This may be due to the organic matter and/or metallic pollution in the sediment, which could influence the hydration reaction of CSA [58]. Even the type of CSA cement may decide its different strength performance [44]. Indeed, the compressive strength of solidified sediments with CSA still can be reached to 78.41 - 98.42 % that of using OPC in this study. Thus, considering the main advantages of CSA - green, low carbon, environmentally

330 friendly, and energy saving, we still consider CSA as an effective alternative for
331 solidification of sediments to replace traditional binder OPC.
332

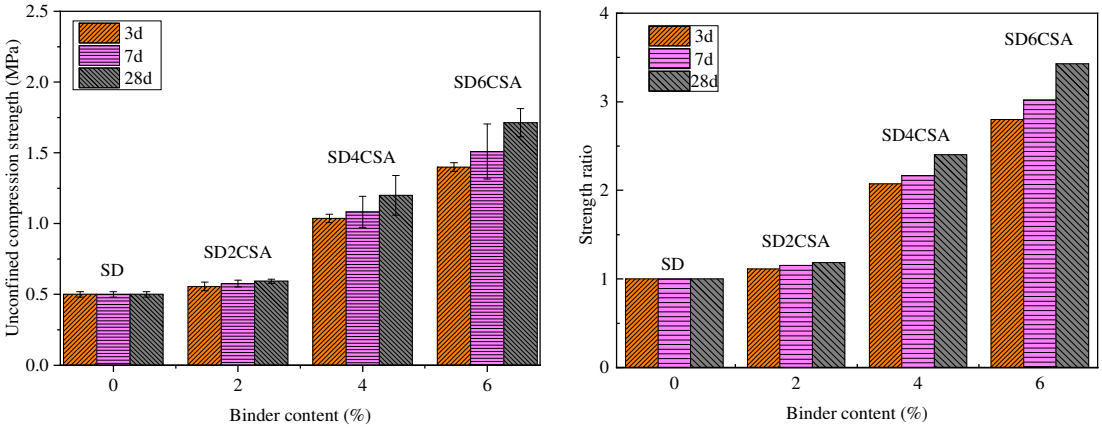

333
334 (a) (b)

335 **Fig. 6.** (a) Unconfined compressive strength and (b) strength ratio of solidified
336 sediments with CSA.
337

338 **3.4. Elastic modulus and secant modulus**

339 Elastic modulus is an important characteristic to evaluate the ability of solidified
340 sediments to resist deformation. As illustrated in Fig. 7, a typical stress-strain curve
341 showing how to determine elastic modulus. It is evident that this typical stress-strain
342 curve can be divided into three stages: (I): initial elastic deformation stage; (II):
343 plastic deformation stage; (III): post-failure stage. The elastic modulus (E) can be
344 obtained from the linear portion (stage I) of the stress-strain curves at 30% of peak
345 stress [55]. Each result consisted of three measurements.
346

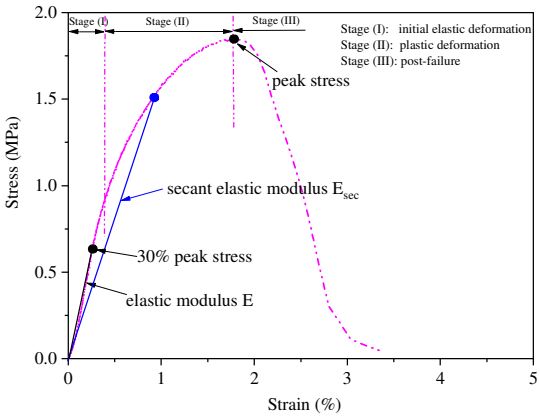

Fig. 7. A determined example of elastic modulus and secant modulus in a typical stress-strain curve.

The variations of elastic modulus E and their error bars of solidified sediments with different binder contents and curing time are plotted in Fig. 8. The results presented indicate that the variation in the elastic modulus has an upward trend as the increase of binder content and the curing time. After 28 d of curing, the elastic modulus of OPC-solidified sediments increases by 2.33 times (0.50 GPa), 7.87 times (1.33 GPa) and 8.53 times (1.43 GPa) as compared with raw sediment (0.15 GPa), with increasing OPC content from 2 % to 6 %. Additionally, the SD4OPC specimen has a higher E values after 7 d and 28 d curing than that at 3 d curing time, E changed from 0.76 GPa (3 d) to 1.18 GPa (7 d) and 1.33 GPa (28 d). A similar conclusion can be observed for CSA-solidified sediment specimens, and both CSA content and curing time had a great influence on the elastic modulus. Higher CSA content and longer curing time benefit for the developing of elastic modulus, such as the specimens cured 28 d, they achieved the higher E values of 0.41 GPa (SD2CSA), 0.86 GPa (SD4CSA) and 1.07 GPa (SD6CSA) when the CSA contents were 2 %, 4 % and 6 %, respectively,

while the E values was only 0.15 GPa for SD. Besides, with the curing time increase from 3 d to 28 d, the E values of CSA-solidified sediment samples were increases significantly, the E values of SD4CSA still as high as 0.64 GPa (3 d), 0.77 GPa (7 d) and 0.86 GPa (28 d). Achour et al. [59] also reported similar conclusions, elastic modulus increases with the increase of binder content and curing time.

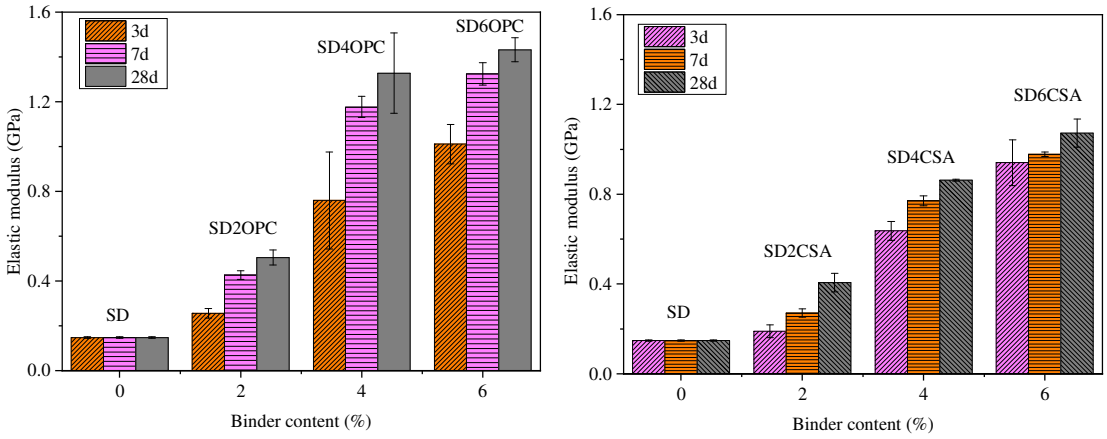

Fig. 8. Elastic modulus of solidified sediments with (a) OPC; (b) CSA.

As showed in Fig. 7, the secant modulus (E_{sec}) was determined from the slope of the lines, which were drawn from the starting point, up to every point of the stress-strain curves [60], [61]. Fig. 9 (a)-(b) shows the secant modulus E_{sec}-strain curves of OPC and CSA-solidified sediments after 28 d cured, respectively. The E_{sec}-strain curves of SD4OPC and SD4CSA at 3 d, 7 d and 28 d are shown in Fig. 9 (c)-(d). From the obtained results, the dominant trend observed of all specimens goes through three stages, which corresponding to the three stages of the stress-strain curves.

(i) Stage I, which corresponding to the initial elastic deformation stage of stress-strain

383 curves, E_{sec} increases a little at low strains in this stage. It is worth to note that E_{sec}
384 should be constant in this stage due to the stress increases linearly with the strain in
385 the initial elastic deformation stage, theoretically. However, because of the contact
386 between specimen and press machine is incomplete at the initial stage, resulting in the
387 stress increases approximately linear with the strain in the experiment, this is the
388 reason that E_{sec} increases a little at low strains in this stage.
389 (ii) Stage II, E_{sec} decreases by the increases of axial strain until the point that
390 corresponding to the peak stress point of stress-strain curves, therefore, it was
391 considered corresponding to the plastic deformation stage of stress-strain curves.
392 (iii) Stage III, which means the post-failure stage of stress-strain curves, E_{sec} sudden
393 decrease significantly with increases of the strain.
394 However, E_{sec} becomes larger for solidified sediments with binder than raw sediments,
395 the higher the binder amount and curing time, the higher the E_{sec} at the same strain.
396 The reason for this event can be explained as the hydration reaction of binder, as the
397 reaction goes on with more binder amount and curing time, the systems produced a
398 large number of hydration products, include the sample particles interact with each
399 other, increase the E_{sec}.
400 It should be noted that the values of elastic modulus and secant modulus differ by an
401 order of magnitude (GPa and MPa). This is because the axial deformation data of the
402 elastic modulus tests comes from three displacement sensors, which were stuck on to
403 the specimens to record the true axial deformation of the specimens. However, the
404 axial deformation data used for the calculation of the secant modulus tests comes

from the press machine; the measured axial deformation of the top and bottom surfaces is greater than the actual axial deformation of the specimen, lead to measured secant modulus much smaller than the true elastic modulus of the specimen. This is also why European standard NF EN 13286-43 [55] recommends this method to measure the true elastic modulus of the specimen.

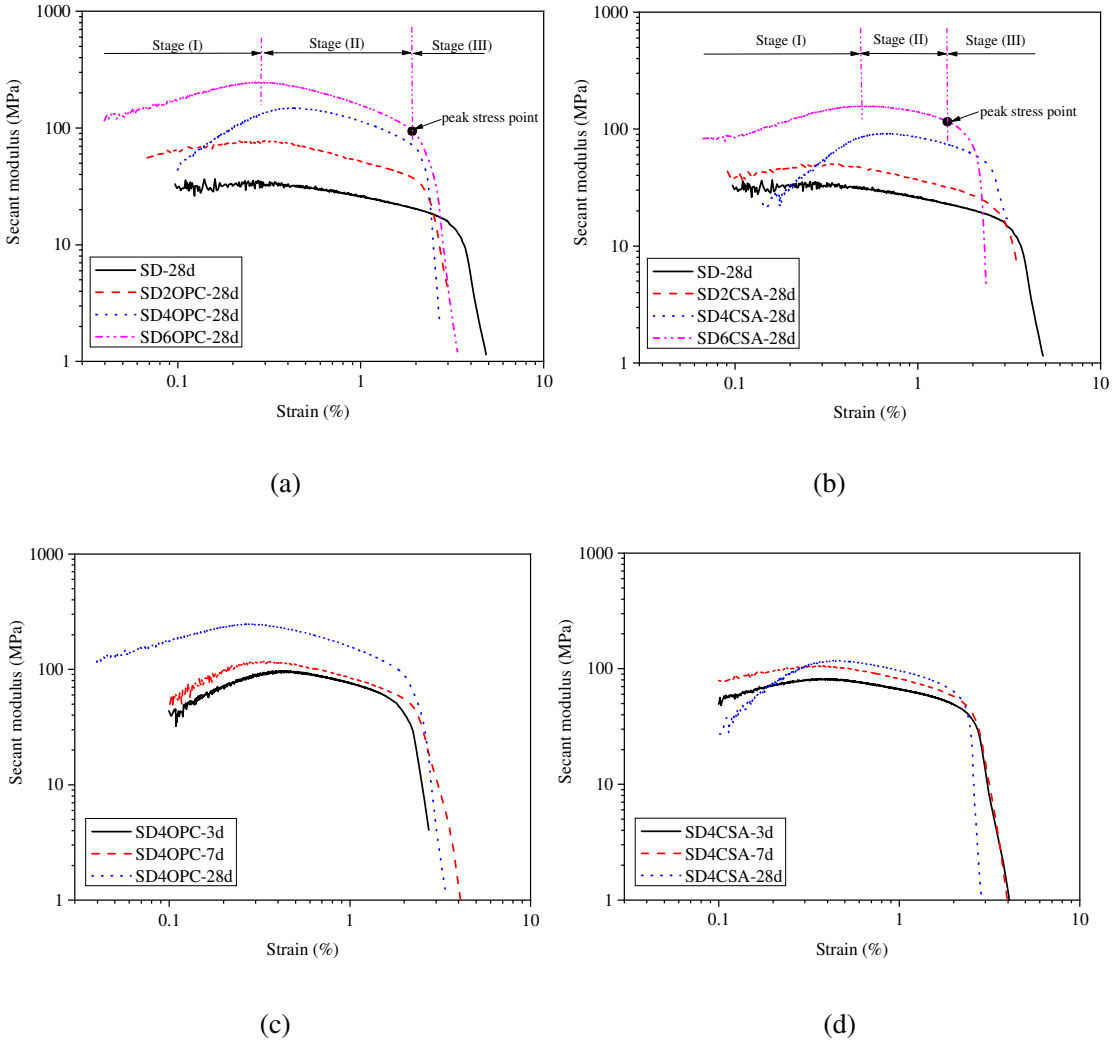

Fig. 9. Secant modulus curves of solidified sediments (a) Sediments with OPC cured 28 d; (b) Sediments with CSA cured 28 d; (c) SD4OPC cured for 3 d, 7 d, and 28 d; (d) SD4CSA cured for 3 d, 7 d, and 28 d.

418

419 **3.5. Splitting tensile strength**

420 Fig. 10 summarizes the effect of binder content and curing time in terms of the
421 splitting tensile force-displacement behavior of solidified sediments. In general, the
422 results reveal some common features: all the curves indicate a brittle behavior, no
423 matter of raw sediment or solidified sediments; the force increases immediately with
424 increasing displacement until reaching the peak splitting tensile force value, then
425 reduce immediately followed by an increase of the displacement.

426 Indeed the peak tensile force and stiffness increase significantly with the increase of
427 binder content and curing time. For 28 d curing specimens, the peak tensile force of
428 SD is 436.54 N, the peak tensile force of solidified sediments increase to 610.41 N
429 (SD2OPC), 1214.26 N (SD4OPC) and 1427.41 N (SD6OPC), due to the addition of
430 2 %, 4 % and 6 % OPC binder. Moreover, the addition of 2 %, 4 % and 6 % CSA
431 binder to the sediments increases the peak tensile force to 453.01 N (SD2CSA),
432 869.69 N (SD4CSA) and 934.21 N (SD6CSA) in relation to the raw sediments after
433 28 d curing. For SD4OPC (Fig. 10c) and SD4CSA (Fig. 10d), it seems that the peak
434 tensile force increase significantly with curing time increase from 3 d to 28 d. The
435 peak tensile force increases to 482.39 N (3 d), 558.00 N (7 d) and 1200.82 N (28 d)
436 for SD4OPC and to 651.08 N (3 d), 786.05 N (7 d) and 914.69 N (28 d) for SD4CSA.

437

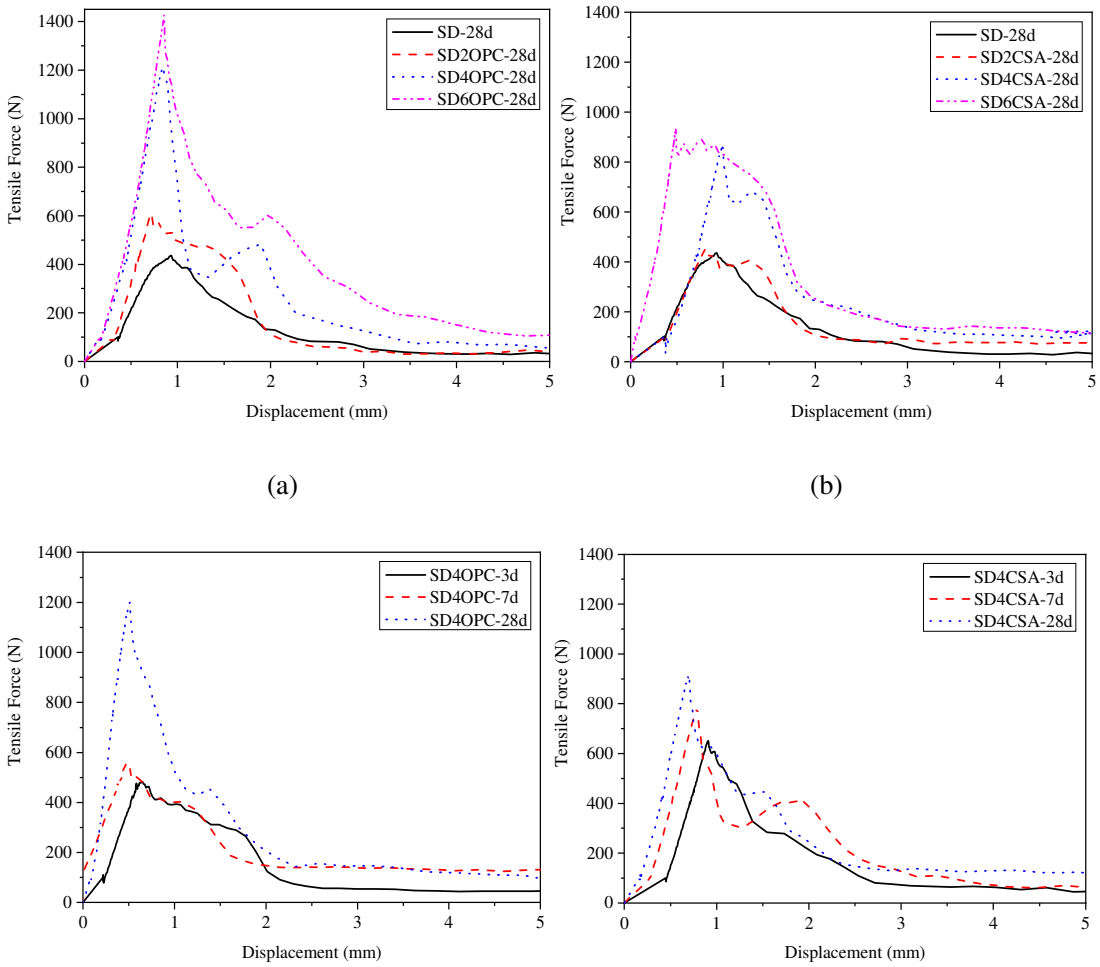

Fig. 10. Splitting tensile force-displacement curves of solidified sediments (a) Sediments with OPC cured 28 d; (b) Sediments with CSA cured 28 d; (c) SD4OPC cured for 3 d, 7 d, and 28 d; (d) SD4CSA cured for 3 d, 7 d, and 28 d.

Fig. 11 shows the variation of the splitting tensile strength (q_{it}) and the tensile strength ratio (η_{it}, defined as the ratio splitting tensile strength of solidified sediment q_{itn} to the splitting tensile strength of raw sediment q_{it0} as shown on Equation (5)) with the amount of binder treatment and curing time.

$$\eta_{it} = \frac{q_{itn}}{q_{ito}} \qquad (5)$$

It can be observed that the OPC inclusion contributes to the enhancement of the splitting tensile strength of solidified sediments. In the same curing time of 28 d, the splitting tensile strength q_{it} increases from 0.050 MPa (SD) to 0.077 MPa (SD2OPC), 0.162 MPa (SD4OPC) and 0.192 MPa (SD6OPC) with the increase of OPC content from 0 % to 6 %, the η_{it} correspondingly increases to 1.54 (SD2OPC), 3.24 (SD4OPC) and 3.84 (SD6OPC) as compared with that of SD (1.00). Moreover, the increase of curing time can effectively improve the q_{it} and η_{it} of the solidified sediments with OPC. The splitting tensile strength of SD4OPC specimen increases to 0.109 MPa (7 d) and 0.162 MPa (28 d) as compared with that at 3 d (0.104 MPa), meanwhile, the corresponding η_{it} changes to 2.18 and 3.24 as compared with that of SD4OPC specimen at 3 d (2.08).

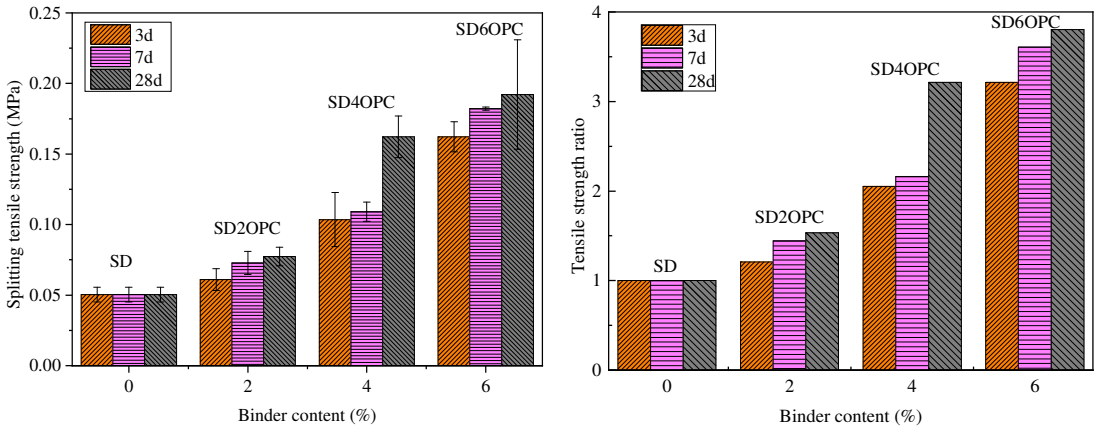

(a) (b)

Fig. 11. (a) Splitting tensile strength and (b) tensile strength ratio of solidified sediments with OPC.

Fig. 12 shows the splitting tensile strength values and tensile strength ratio of

CSA-solidified sediments specimens cured for 3 d, 7 d and 28 d. As expected, the CSA has an obviously positive effect on the tensile strength during all times. This is because the CSA with water systems produced a large number of hydration products, which are formed filled pores to give a higher strength.

Especially for the specimens with 2, 4 and 6 % CSA at 28 d, which had the higher tensile strength of 0.057 MPa, 0.114 MPa and 0.119 MPa than that of SD (0.050 MPa), and the η_{it} correspondingly is 1.14 (SD2OPC), 2.28 (SD4OPC), 2.38 (SD6OPC) and 1.00 (SD). This indicated that the addition of CSA could significantly improve the tensile strength of the solidified sediments. As the reaction proceeds, there was an increase in tensile strength for SD4CSA specimens after cured, and the tensile strength achieved the most about 0.082 MPa, 0.100 MPa and 0.114 MPa at 3 d, 7 d and 28 d, respectively, while the η_{it} correspondingly is 1.64 (3 d), 2.00 (7 d) and 2.28 (28 d). According to the research of Zhang et al. [62], the ettringite is the main hydration product and plays a significant role in improving the strength of CSA treated specimens, and ettringite continues to increase with curing time and CSA content. Thus, this is the reason that the splitting tensile strength of CSA-solidified sediment specimens increases with the increasing of curing time and CSA content.

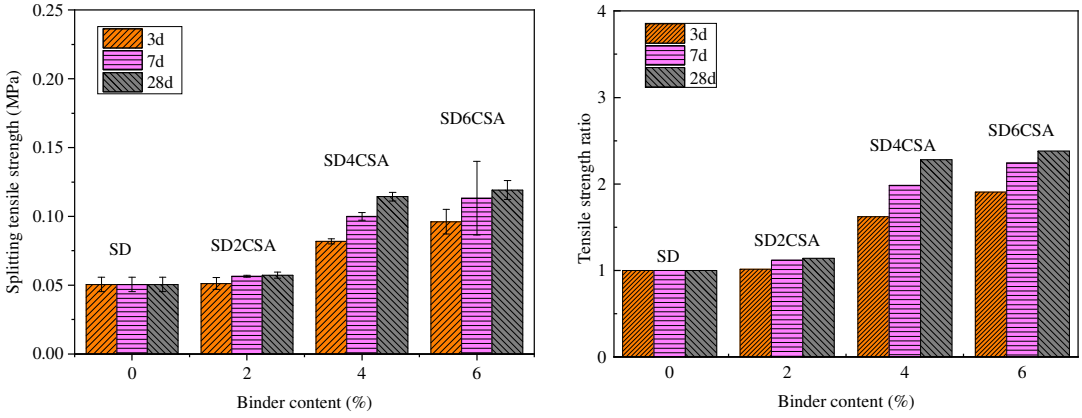

(a) (b)

Fig. 12. (a) Splitting tensile strength and (b) tensile strength ratio of solidified sediments with CSA.

3.6. Relationship of mechanic parameters q_c, q_{it} and E

In this study, a regression analysis was performed on the relationship between the compressive and tensile splitting strengths values, as shown in Fig 13 (a). Based on this figure, a simple linear model has been used for describing the relationship between the compressive and tensile splitting strengths of solidified sediments. Equations (6)-(7) have been derived for describing the relationship between the compressive and splitting strength of OPC solidified sediments and CSA solidified sediments in this study.

$$q_c = 9.5 q_{it} \quad (6)$$

$$q_c = 12.2 q_{it} \quad (7)$$

These equations are plotted in Fig. 13 (a) with the experimental data. It can be seen that the regression lines from equations (6)-(7) showed a relatively good relationship between the compressive and splitting strength. The coefficient of determination (R^2),

506 which indicates how much of the total variation in the dependent variable can be
507 accounted for by the regression equation, was obtained as 0.99 and 0.98 for equations
508 (6)-(7) in this study, respectively. In particular, it is found that a unified equation (8)
509 with R^2 = 0.97 can satisfactorily describe the correlation between q_c and q_{it} on all
510 solidified sediment specimens. Therefore, the derived linear equations may
511 successfully be used to represent the relationship between the compressive and
512 splitting strength of solidified sediments.

513 $$q_c = 10.4 q_{it} \quad (8)$$

514 Fig 13 (b)-(c) show the variation of compressive strength q_c versus elastic modulus E
515 and splitting tensile strength q_{it} versus elastic modulus E, respectively. It is observed
516 that both q_c and q_{it} have a trend to increase with the increasing E according to the
517 obtained test data points. In this study, the simple exponential model was used for
518 describing the relationship between the strength and elastic modulus. The model
519 results between q_c and E of OPC- and CSA-solidified sediments are reflected in
520 equation (9) and (10) with the coefficient of determination R^2 = 0.93 and 0.98,
521 respectively. The unified equation (11) with R^2 = 0.92 can explain how compressive
522 strength is related to the elastic modulus of solidified sediment specimens.

523 $$q_c = 0.471 e^{0.931E} \quad (9)$$

524 $$q_c = 0.407 e^{1.313E} \quad (10)$$

525 $$q_c = 0.454 e^{1.040E} \quad (11)$$

526 Equation (12) and (13) with R^2 = 0.94 and 0.95, respectively, are derived from the
527 regression analysis to express quantitatively the correlation of q_{it} and E of OPC- and

CSA-solidified sediments. A unified equation can be expressed by equation (14) with R^2 = 0.94, which can be acceptable to describe approximately the changing trend of splitting strength with elastic modulus on the designed materials.

$$q_{it} = 0.046e^{0.997E} \quad (12)$$

$$q_{it} = 0.043e^{0.990E} \quad (13)$$

$$q_{it} = 0.044e^{1.011E} \quad (14)$$

In general, equation (8), (11) and (14) demonstrates the relationships among the compressive strength, tensile strength and elastic modulus, this is to say, these equations provide an alternative approach to predict the approximate value of other two parameters if one parameter is given. By example, this leads to help to predict the tensile strength and the elastic modulus from the compression strength. This later test is easier to perform, cheaper and quicker to carry out in comparison to the tensile strength and the elastic modulus measurements. Moreover, in the stage of designing a new formulation, this procedure could save time, reduce the number of samples and hence save the materials. Even if the ratio of 10 between the compressive strength over the tensile strength is commonly encountered for OPC treated materials, the relation between the tensile strength or the compressive strength with the young modulus has to be specific to a given material (in our case to treated sediments).

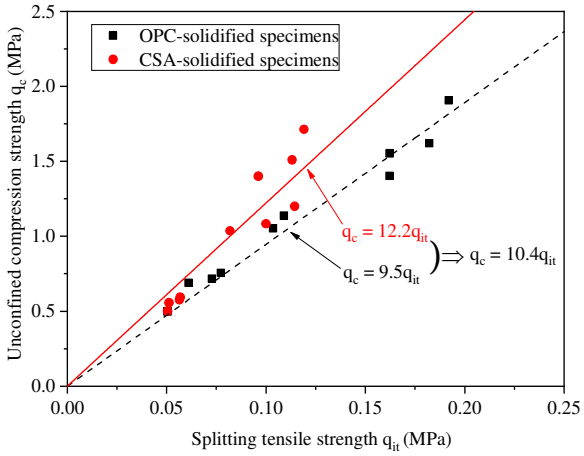

(a)

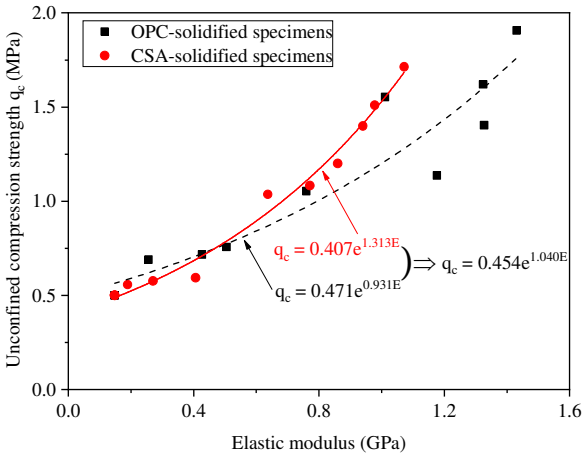

(b)

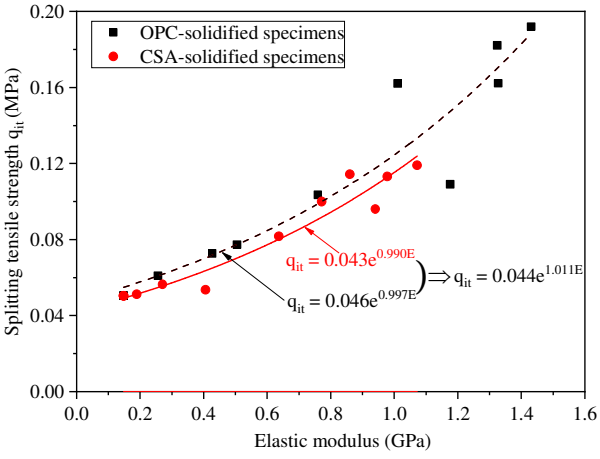

(c)

Fig. 13. Relationship of (a) compression and splitting tensile strength; (b) compression strength and elastic modulus; (c) splitting tensile strength and elastic modulus.

3.7 Evaluation of solidified sediments as road materials

Fig. 14 assess the suitability of solidified dredged sediments as road materials according to European standard NF EN 14227-15 [63], using the mechanical characteristics of the direct tensile strength (q_t) and elastic modulus (E) at 360 d of the solidified dredged sediments.

It is noted that the direct tensile strength q_t shall be derived from q_{it} using the Equations (15) [56] [63]. The estimated values at 360 d for solidified sediments with cement should be calculated from the measured values at the curing period of 28 d, according to Equations (16) and (17) [8] [59]. In the absence of specific data, the coefficients 0.6 and 0.65 are assumed to remain valid for solidified sediments. The use of this extrapolation was confirmed in the literature. The results from Wang et al. [8] and Achour et al. [59] confirmed this extrapolation.

$$q_t = 0.8 q_{it} \quad (15).$$

$$\frac{q_t - 28d}{q_t - 360d} = 0.6 \quad (16)$$

$$\frac{E - 28d}{E - 360d} = 0.65 \quad (17)$$

However, a great improvement of material classification can be observed, compared with raw sediments. This proves the beneficial effects of OPC and CSA treatment to increase the mechanical properties of raw sediments. It should be noted that the minimum class required for potential use as a sub-base material in class T2. Hence, this means that no samples in this study can be used as a sub-base or base course material for a large class of traffic intensities. The samples of SD4OPC and SD6OPC,

578 which belong to the class T1 might be possibly reused as roadbed filling materials for
579 roads of low traffic intensity. This conclusion is consistent with the previous study [8].
580 If the need arises to enhance the material classification to Class T2 for high traffic
581 intensity, the effective way may be to increase the amount of binder and/or to explore
582 the combined effect of OPC and CSA, finally to combine the present sediments with
583 coarser materials to improve its mechanical properties. This work will be carried out
584 in a next stage.

585

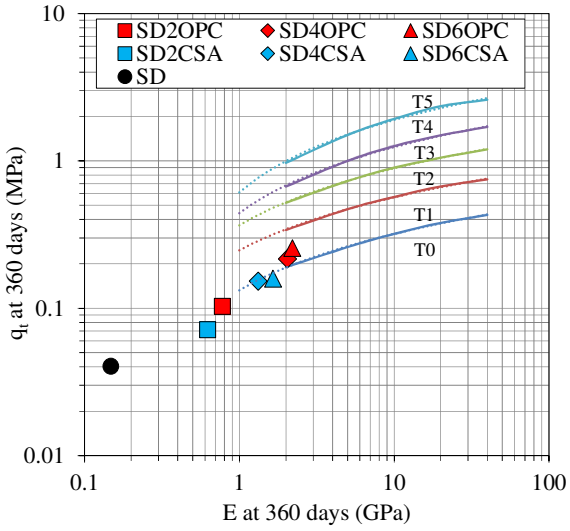

586

587 **Fig. 14.** Classification of solidified sediments with OPC and CSA.

588

589 **3.8 X-ray diffraction analysis**

590 X-ray diffraction (XRD) analysis was used to determine the mineralogical
591 composition of raw and OPC/CSA-solidified sediments at 7d, and the representative
592 results are given in Fig. 15. For raw sediments, quartz (SiO_2) and calcite ($CaCO_3$)
593 were observed as the main phases, the result also indicated some minor phases such as
594 gypsum ($CaSO_4$), kaolinite, muscovite, microcline, and albite. The main hydration

595 phases observed of OPC-solidified sediments (SD6OPC) are portlandite ($CaOH_2$) and
596 a little of ettringite ($Ca_6Al_2S_3O_{50}H_{64}$), however, calcium silicate, calcium aluminate
597 and aluminosilicate phases were not detected. XRD results reveal that the ettringite
598 ($Ca_6Al_2S_3O_{50}H_{64}$) is the main hydration product in CSA-solidified sediments
599 (SD6CSA). The XRD results show the different main hydration product for OPC and
600 CSA-solidified sediments, lead to the different mechanical strength of solidified
601 sediments.

602

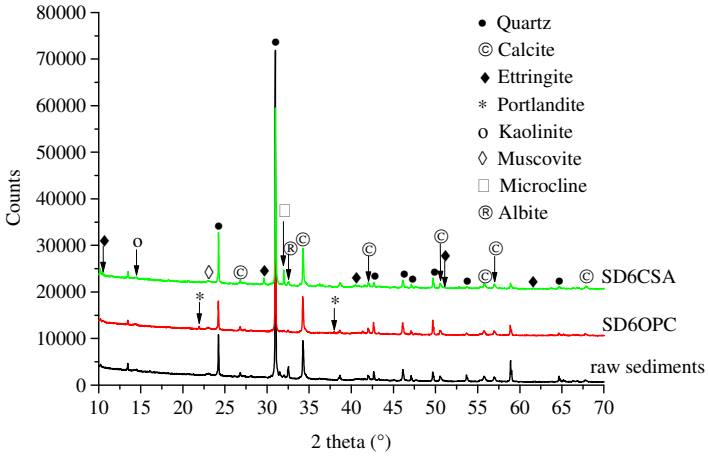

603

604 **Fig. 15.** XRD traces of raw sediments, OPC-solidified sediments and CSA-solidified
605 sediments specimens.

606

607 **3.9 Micropore structure analysis**

608 The micropore structure of the solidified sediments was investigated and the results is
609 shown in Fig. 16 and Table 4. It's easily observed that the four typical samples
610 showed approximately the same pattern with apparent diameters of pores in the range
611 of 0.006-400 μm, and all the pore size distributions model are bimodal. Indeed, the
612 main pores of all the samples distributed in the range of 0.01–1.0 μm and 1.0–40 μm.

According to previous research [64], the pore structure can be divided into four major ranges: <0.01 μm, 0.01-1 μm, 1-40 μm and >40 μm, as presented in Table 4. With the curing time increase from 3 d to 7 d, the pores volume percentage of larger pores in the range of 1-40 μm and >40 μm shows a decreasing trend, while the pores volume percentage of the smaller pores in the range of <0.01μm and 0.01-1 μm shows an increasing trend. This is due probably to the progress of hydration of binders, which causes that the larger pores (1-40 μm and >40 μm) transform to smaller pores (<0.01μm and 0.01-1μm), which induces that the pores of the solidified sediments became finer and denser.

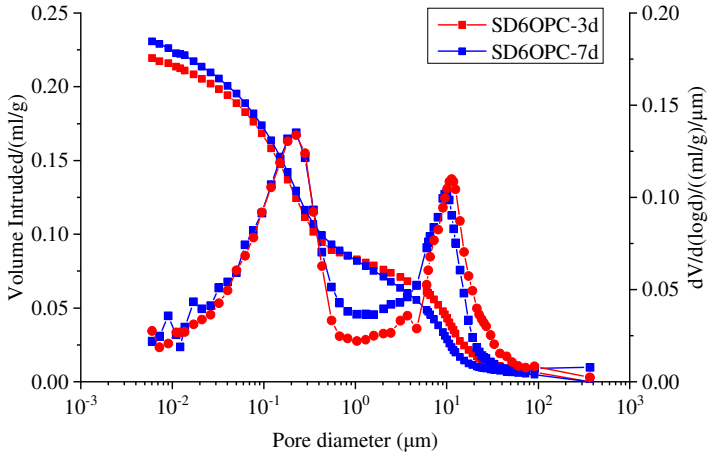

(a)

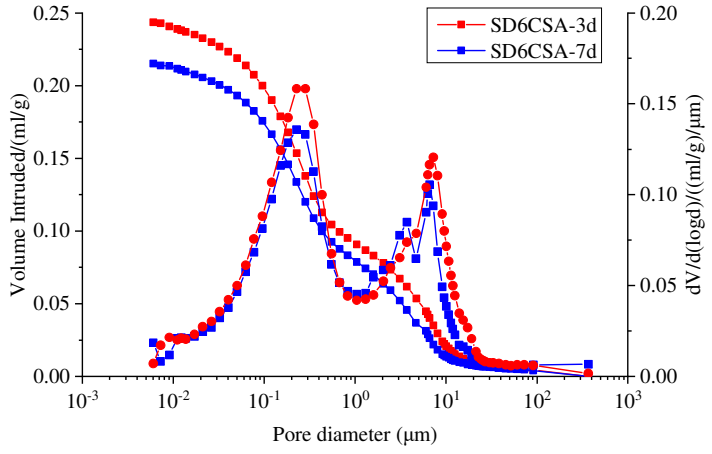

(b)

Fig. 16. Micropore structure analysis of (a) OPC-solidified sediments and (b) and CSA-solidified sediments.

Table 4 Pore size distribution of the solidified sediments

Pore size (μm)	Pore size distribution (%)			
	SD6CSA-3d	SD6CSA-7d	SD6OPC-3d	SD6OPC-7d
>40	2.80	2.72	4.72	3.18
1-40	34.51	33.88	33.12	32.30
0.01-1	60.78	61.82	59.53	61.06
<0.01	1.91	1.57	2.63	3.45
Total	100	100	100	100

4. Conclusion

In this study, a series of experiments were performed to clarify the feasibility of recycling dredged marine sediments with novel eco-binder CSA cement as road construction materials. The results are compared with the OPC treated sediments. Based on the obtained results, the following conclusions can be drawn:

(1) Compared with the raw sediments, the compaction performance of the solidified sediments is significantly improved, which reflects the behavior improvement of solidified sediment in a short time that curing for less than 1 hour. The increase in the I-CBR index value is almost linear with the increase of the binder content (at least in the range of binder content studied in this work). In terms of maximum dry density and the optimum moisture of solidified sediment:

a. For OPC treatment, the maximum dry density is decreased

accompanied by increasing optimal water content.

b. For CSA treatment, after the first decrease of the treatment with 2 % CSA, an increase in maximum dry density is observed for higher treatment content. In the same way, after an increase in the optimal water content of the treatment with 2 % CSA, a decrease is observed for higher treatment content.

(2) The incorporation of binder in raw sediments is effective for the improvement in mechanic behavior of solidified sediment in the long term that curing for several days or even longer periods, includes compressive strength, tensile strength and elastic modulus, and these mechanical parameters increase with binder content and curing time.

(3) A relative evaluation of the effectiveness of treatment with OPC and CSA has revealed that CSA increases relatively the mechanical properties of solidified sediments in the early stage (during the first three days). Whereas OPC shows a marked increase between 3 d and 28 d.

(4) The simple model can satisfactorily describe, respectively, the relationships among the compressive strength, tensile strength and elastic modulus; these equations provide an alternative approach to predict the approximate value of two parameters if the one parameter is given. Which leads to reduce the number and time of the experiments. It is to note that the relation between the strength and the elastic modulus is material dependent.

(5) The microstructure induced by OPC treatment and CSA treatment seems to be

comparable. The pore size distribution induced is of type bimodal.

(6) The evaluation of solidified sediment classification confirms that valorization sediment in road materials is entirely possible.

Acknowledgements

The authors would like to thank the financial support of the National Natural Science Foundation of China (Grant no. 51879202, Grant no. 52079098) and China Scholarship Council. The authors would also like to thank the support of IMT Lille Douai.

675 **References**

676 [1] EuDA (European Dredging Association), Dredged Material & Environmental
677 Regulations in EU, 2005.

678 [2] T. N. Burt, Guidelines for the beneficial use of dredged material. Technical Report.
679 HR Wallingford, 1996.

680 [3] D. Xu, M. Huang, Y. Zhou. One-dimensional compression behavior of calcareous
681 sand and marine clay mixtures. Int. J. Geomech. 20(9) (2020) 04020137.

682 [4] M. A. Ross, A. J. Mehta, On the mechanics of lutoclines and fluid mud. J Coast
683 Res. (1989) 51-62.

684 [5] D. Xu, X. Xu, W. Li, B. Fatahi. Field experiments on laterally loaded piles for an
685 offshore wind farm. Mar. Struct. 69 (2020) 102684.

686 [6] A. R. Wiegman, J. W. Day, C. F. D'Elia, J. S. Rutherford, J. T. Morris, E. D. Roy, ...
687 & B. F. Snyder. Modeling impacts of sea-level rise, oil price, and management
688 strategy on the costs of sustaining Mississippi delta marshes with hydraulic dredging.
689 Sci. Total Environ. 618 (2018) 1547-1559.

690 [7] N. Harikrishnan, R. Ravisankar, A. Chandrasekaran, M. S. Gandhi, K. V.
691 Kanagasabapathy, M. V. R. Prasad, & K. K. Satapathy. Assessment of heavy metal
692 contamination in marine sediments of east coast of Tamil Nadu affected by different
693 pollution sources. Mar. Pollut. Bull. 121 (1-2) (2017) 418-424.

694 [8] R. Zentar, D. Wang, N. E. Abriak, M. Benzerzour, W. Chen. Utilization of
695 siliceous–aluminous fly ash and cement for solidification of marine sediments. Constr
696 Build Mater. 35 (2012) 856-863.

697 [9] D. Wang, N. E. Abriak, R. Zentar. Strength and deformation properties of Dunkirk
698 marine sediments solidified with cement, lime and fly ash. Eng Geol. 166 (2013)
699 90-99.
700 [10] V. Dubois, N. E. Abriak, R. Zentar, G. Ballivy. The use of marine sediments as a
701 pavement base material. Waste Manage. 29 (2) (2009) 774-782.
702 [11] D. Wang, N. E. Abriak, R. Zentar, W. Xu. Solidification/stabilization of dredged
703 marine sediments for road construction. Environ. Technol., 33 (1) (2012) 95-101.
704 [12] D. Wang, R. Wang, M. Benzerzour, H. Wang, N. E. Abriak. Comparison between
705 reactive MgO- and Na2SO4-activated low-calcium fly ash solidified soils dredged
706 from East Lake, China. Mar Georesour Geotec. 38(9) (2020) 1046-1055.
707 [13] W. Maherzi, M. Benzerzour, Y. Mamindy-Pajany, E. van Veen, M. Boutouil, N. E.
708 Abriak. Beneficial reuse of Brest-Harbor (France)-dredged sediment as alternative
709 material in road building: laboratory investigations. Environ. Technol. 39 (5) (2018)
710 566-580.
711 [14] M. Taneez, N. Marmier, C. Hurel. Use of neutralized industrial residue to
712 stabilize trace elements (Cu, Cd, Zn, As, Mo, and Cr) in marine dredged sediment
713 from South-East of France. Chemosphere. 150 (2016) 116-122.
714 [15] L. Wang, J. S. Kwok, D. C. Tsang, C. S. Poon. Mixture design and treatment
715 methods for recycling contaminated sediment. J. Hazard. Mater. 283 (2015) 623-632.
716 [16] L. Wang, L. Chen, D. W. Cho, D. C. Tsang, J. Yang, D. Hou, ... C. S. Poon. Novel
717 synergy of Si-rich minerals and reactive MgO for stabilisation/solidification of
718 contaminated sediment. J. Hazard. Mater. 365 (2019) 695-706.

719 [17] L. Wang, L. Chen, D. C. Tsang, J. S. Li, T. L. Yeung, S. Ding, & C. S. Poon.
720 Green remediation of contaminated sediment by stabilization/solidification with
721 industrial by-products and CO_2 utilization. Sci. Total Environ. 631 (2018), 1321-1327.
722 [18] D. D. Higgins, GGBS and Sustainability. Proceedings of the Institution of Civil
723 Engineers - Construction Materials 160 (3) (2007) 99-101.
724 [19] N. T. Dung, C. Unluer. Carbonated MgO concrete with improved performance:
725 the influence of temperature and hydration agent on hydration, carbonation and
726 strength gain. Cem Concr Compos. 82 (2017) 152-164.
727 [20] J. L. Provis. Green concrete or red herring?–future of alkali-activated materials.
728 Adv. Appl. Ceram. 113 (8) (2014) 472-477.
729 [21] D. Wang, H. Wang, X. Wang. Compressibility and strength behavior of marine
730 soils solidified with MgO—A green and low carbon binder. Mar Georesour Geotec.
731 35(6) (2017), 878-886.
732 [22] D. Wang, H. Wang, S. Di. Mechanical properties and microstructure of
733 magnesia–fly ash pastes. Road Mater. Pavement Des. 20 (5) (2019) 1243-1254.
734 [23] D. Wang, H. Wang, Y. Jiang. Water immersion-induced strength performance of
735 solidified soils with reactive MgO—A green and low carbon binder. J. Test. Eval. 47
736 (2) (2019) 1569-1585.
737 [24] D. Wang, X. Gao, R. Wang, S. Larsson, M. Benzerzour. Elevated curing
738 temperature-associated strength and mechanisms of reactive MgO-activated industrial
739 by-products solidified soils. Mar Georesour Geotec. 38(6) (2020) 659-671.
740 [25] C. Van Bunderen, R. Snellings, L. Vandewalle, Ö. Cizer. Early-age hydration and

741 autogenous deformation of cement paste containing flash calcined dredging sediments.
742 Constr Build Mater. 200 (2019) 104-115.
743 [26] D. Wang, H. Wang, S. Larsson, M. Benzerzour, W. Maherzi, M. Amar. Effect of
744 basalt fiber inclusion on the mechanical properties and microstructure of
745 cement-solidified kaolinite. Constr Build Mater. 241 (2020), 118085.
746 [27] Z. Zhao, M. Benzerzour, N. E. Abriak, D. Damidot, L. Courard, D. Wang. Use of
747 uncontaminated marine sediments in mortar and concrete by partial substitution of
748 cement. Cem Concr Compos. 93 (2018), 155-162.
749 [28] P. Chaunsali, P. Mondal. Influence of calcium sulfoaluminate (CSA) cement
750 content on expansion and hydration behavior of various ordinary portland cement-
751 CSA blends. J. Am. Ceram. Soc. 98(8) (2015) 2617-2624.
752 [29] F. P. Glasser, L. Zhang. High-performance cement matrices based on calcium
753 sulfoaluminate–belite compositions. Cem Concr Res. 31 (12) (2001).1881-1886.
754 [30] M.C.G. Juenger, F. Winnefeld, J.L. Provis, et al. Advances in alternative
755 cementitious binders. Cem. Concr. Res. 41 (12) (2011) 1232-1243.
756 [31] J. Zhang, G. Li, W. Ye, Y. Chang, Q. Liu, Z. Song. Effects of ordinary Portland
757 cement on the early properties and hydration of calcium sulfoaluminate cement.
758 Constr Build Mater. 186 (2018) 1144-1153.
759 [32] G. Li, J. Zhang, Z. Song, C. Shi, A. Zhang. Improvement of workability and early
760 strength of calcium sulphoaluminate cement at various temperature by chemical
761 admixtures. Constr Build Mater. 160 (2018) 427-439.
762 [33] F.P. Glasser, L. Zhang. High-performance cement matrices based on calcium

763 sulfoaluminate - belite compositions Cem. Concr. Res. 31 (2001) 1881-1886.
764 [34] J.G. Cabrera, A.S. Al-Hasan. Performance properties of concrete repair materials
765 Constr. Build. Mater. 11 (5–6) (1997) 283-290.
766 [35] Z. Ge, H. Yuan, R. Sun, H. Zhang, W. Wang, H. Qi. Use of green calcium
767 sulphoaluminate cement to prepare foamed concrete for road embankment: A
768 feasibility study. Constr. Build. Mater. 237 (2020) 117791.
769 [36] J. P. Won, J. M. Kim, S. J. Lee, S. W. Lee, S. K. Park. Mix proportion of
770 high-strength, roller-compacted, latex-modified rapid-set concrete for rapid road
771 repair. Constr. Build. Mater. 25 (4) (2011) 1796-1800.
772 [37] C. C. D. Coumes, S. Courtois, S. Peysson, J. Ambroise, J. Pera. Calcium
773 sulfoaluminate cement blended with OPC: A potential binder to encapsulate low-level
774 radioactive slurries of complex chemistry. Cem Concr Res. 39 (9) (2009) 740-747.
775 [38] C. A. Luz, J. Pera, M. Cheriaf, J. C. Rocha. Behaviour of calcium sulfoaluminate
776 cement in presence of high concentrations of chromium salts. Cem Concr Res. 37 (4)
777 (2007) 624-629.
778 [39] R. C. Ivanov, C. A. da Luz, H. E. Zorel Jr, J. I. Pereira Filho. Behavior of calcium
779 aluminate cement (CAC) in the presence of hexavalent chromium. Cem Concr
780 Compos. 73 (2016) 114-122.
781 [40] X. Sun, W. Zhu, X. Qian, Z. Xu. Exploring cementitious additives for
782 pretreatment of high-early-strength sewage sludge from the perspective of the rapid
783 generation of nonevaporable water. J. Mater. Civ. Eng. 26 (5) (2013) 878-885.
784 [41] C. A. Luz, J. C. Rocha, M. Cheriaf, J. Pera. Use of sulfoaluminate cement and

785 bottom ash in the solidification/stabilization of galvanic sludge. J. Hazard. Mater. 136
786 (3) (2006) 837-845.
787 [42] S. Subramanian, Q. Khan, T. Ku. Strength development and prediction of
788 calcium sulfoaluminate treated sand with optimized gypsum for replacing OPC in
789 ground improvement. Constr Build Mater. 202 (2019) 308-318.
790 [43] S. Subramanian, S. W. Moon, J. Moon, T. Ku. CSA-treated sand for geotechnical
791 application: microstructure analysis and rapid strength development. J. Mater. Civ.
792 Eng. 30(12) (2018) 04018313.
793 [44] G. Vinoth, S. W. Moon, J. Moon, T. Ku. Early strength development in
794 cement-treated sand using low-carbon rapid-hardening cements. Soils Found. 58(5)
795 (2018) 1200-1211.
796 [45] S. W. Moon, G. Vinoth, S. Subramanian, J. Kim, T. Ku. Effect of fine particles on
797 strength and stiffness of cement treated sand. Granul Matter. 22(1) (2020) 9.
798 [46] AFNOR (Association Française de Normalization). (1995). Soils: Investigation
799 and testing—Determination of the water content of materials—Oven drying method.
800 NF P94 050, Paris, France: AFNOR.
801 [47] CEN (European Committee for Standardization). (2015). Geotechnical
802 investigation and testing - Laboratory testing of soil - Part 3: determination of particle
803 density. ISO 17892-3. Brussels, Belgium: CEN.
804 [48] AFNOR (Association Française de Normalization). (1998). Soils: Investigation
805 and testing—Determination of the organic matter content—Ignition method. NF P94
806 047, Paris, France: AFNOR.

807 [49] CEN (European Committee for Standardization). (2018). Geotechnical
808 investigation and testing - Laboratory testing of soil - Part 12: determination of liquid
809 and plastic limits. EN ISO 17892-12. Brussels, Belgium: CEN.
810 [50] CEN (European Committee for Standardization). (2020). Particle size analysis -
811 Laser diffraction methods. EN ISO 13320 . Brussels, Belgium: CEN.
812 [51] CEN (European Committee for Standardization). (2010). Unbound and
813 hydraulically bound mixtures. Part 2: Test methods for the determination of the
814 laboratory reference density and water content. Proctor compaction. NF EN 13286-2.
815 Brussels, Belgium: CEN.
816 [52] CEN (European Committee for Standardization). (2012). Unbound and
817 hydraulically bound mixtures. Part 47: Test method for the determination of
818 California bearing ratio, immediate bearing index and linear swelling. NF EN
819 13286-47. Brussels, Belgium: CEN.
820 [53] CEN (European Committee for Standardization). (2003). Unbound and
821 hydraulically bound mixtures. Part 41: Test method for the determination of the
822 compressive strength of hydraulically bound mixtures. NF EN 13286-41. Brussels,
823 Belgium: CEN.
824 [54] CEN (European Committee for Standardization). (2005). Unbound and
825 hydraulically bound mixtures. Part 53: Methods for the manufacture of test specimens
826 of hydraulically bound mixtures using axial compression. NF EN 13286-53. Brussels,
827 Belgium: CEN.
828 [55] CEN (European Committee for Standardization). (2003). Unbound and

829 hydraulically bound mixtures. Part 43: Test method for the determination of the
830 modulus of elasticity of hydraulically bound mixtures. NF EN 13286-43. Brussels,
831 Belgium: CEN.
832 [56] CEN (European Committee for Standardization). (2003). Unbound and
833 hydraulically bound mixtures. Part 42: Test method for the determination of the
834 indirect tensile strength of hydraulically bound mixtures. NF EN 13286-42. Brussels,
835 Belgium: CEN.
836 [57] French recommendations, 1998. Assises de chaussées: guide d'application des
837 normes pour le réseau routier national (Road foundations: guide to the application of
838 standards for the national road network).
839 [58] Z. Gu, S. Hua, W. Zhao, S. Li, Z. Gao, H. Shan,. Using alkali-activated
840 cementitious materials to solidify high organic matter content dredged sludge as
841 roadbed material. Adv. Civ. Eng. 2018 (2018).
842 [59] R. Achour, N. E. Abriak, R. Zentar, P. Rivard, P. Gregoire, Valorization of
843 unauthorized sea disposal dredged sediments as a road foundation material. Environ.
844 Technol. 35 (16) (2014) 1997-2007.
845 [60] M. Ghadakpour, A. Janalizadeh Choobbasti, S. Soleimani Kutanaei, Investigation
846 of the deformability properties of fiber reinforced cemented sand. J Adhes Sci Technol.
847 33 (17) (2019) 1913-1938.
848 [61] M. Ghadakpour, A. J. Choobbasti, S. S. Kutanaei, Investigation of the Kenaf 6
849 hybrid length on the properties of the cement-treated sandy soil. Transp. Geotech. 22
850 (2020) 100301.

851 [62] J. Zhang, G. Li, W. Ye, Y. Chang, Q. Liu, Z. Song. Effects of ordinary Portland
852 cement on the early properties and hydration of calcium sulfoaluminate cement.
853 Constr Build Mater. 186 (2018) 1144-1153.
854 [63] CEN (European Committee for Standardization). (2016). Hydraulical bound
855 mixtures. Part 15: Hydraulically stabilized soils. NF EN 14227-15. Brussels, Belgium:
856 CEN.
857 [64] D. Wang, J. Xiao, X. Gao, Strength gain and microstructure of carbonated
858 reactive MgO-fly ash solidified sludge from East Lake, China. Eng Geol. 251 (2019)
859 37-47.